International Journal of Minerals, Metallurgy and Materials
Volume 21, Number 7, July 2014, Page 647
DOI: 10.1007/s12613-014-0953-2

Thermodynamic analysis of the compositional control of inclusions in cutting-wire steel

Jing Zhang[1,2], *Fu-ming Wang*[1,2], *and Chang-rong Li*[3]

1) School of Metallurgical and Ecological Engineering, University of Science and Technology Beijing, Beijing 100083, China
2) State Key Laboratory of Advanced Metallurgy, University of Science and Technology Beijing, Beijing 100083, China
3) School of Materials Science and Engineering, University of Science and Technology Beijing, Beijing 100083, China
(Received: 5 November 2013; revised: 26 December 2013; accepted: 27 December 2013)

Abstract: Data from a thermodynamic database and the calculation software FactSage were used to investigate the phase diagrams of the MnO–CaO–SiO_2–Al_2O_3 system in cutting-wire steel and the effects of oxide components on the low-melting-point (LMP) zone in the corresponding phase diagrams. Furthermore, the activities of oxide components in the quaternary system at an Al_2O_3 content of 25wt% were calculated. The contents of dissolved [Al] and [O] in liquid steel in equilibrium with LMP inclusions in the MnO–CaO–SiO_2–Al_2O_3 system were optimized. The results show that the MnO–CaO–SiO_2–Al_2O_3 system possesses the largest LMP zone (below 1400°C) at an Al_2O_3 content of 25wt% and that the CaO content should be simultaneously controlled in the range of 40wt% to 45wt%. The activities of the oxide components CaO, MnO, and SiO_2 should be restricted in the ranges of 0 to 0.05, 0.01 to 0.6, and 0.001 to 0.8, respectively. To obtain LMP inclusions, the [Al] and [O] contents in cutting-wire steel must be controlled within the ranges of 0.5×10^{-6} to 1.0×10^{-5} and 3.0×10^{-6} to 5.0×10^{-5}, respectively.

Keywords: wire steel; cutting; inclusions; thermodynamic calculations; activity; oxides

1. Introduction

Currently, the compositional control of inclusions has become an important way to produce clean steel in the process of steelmaking, especially in the cases of cutting-wire steel, tire-cord steel, and valve-spring steel [1–2]. Therefore, to reduce the harmful effects caused by brittle inclusions such as aluminum oxide and calcium aluminate, these inclusions should be eliminated or replaced by low-melting-point plastic inclusions that are deformable during hot-rolling. According to Refs. [3–9], the deformability of inclusions is known to be directly related to their melting point and a lower melting point is known to result in a better deformability. Moreover, the authors of several previous studies [10–13] have concentrated on the ternary systems MnO–SiO_2–Al_2O_3 and CaO–SiO_2–Al_2O_3 as well as on the quaternary system CaO–SiO_2–Al_2O_3–MgO in tire-cord steel and have calculated the low-melting-point zones and optimal liquid steel compositions. However, compositional control of inclusions in cutting-wire steel has not been reported. Because Mn/Si deoxidization is an essential way to produce cutting-wire steel, the oxide inclusions formed during the steelmaking process tend to be MnO–CaO–SiO_2–Al_2O_3. In this work, the thermodynamic database and FactSage software are employed to calculate the phase diagrams of the MnO–CaO–SiO_2–Al_2O_3 quaternary system and the activities of the oxide components. More importantly, by combining our calculated results with the experimental results obtained for cutting-wire steel from one steel plant, we optimize the composition of liquid steel in equilibrium with the low-melting-point (LMP) inclusions. All of the thermodynamic calculations performed using the software FactSage are based on the minimization of the total Gibbs energy at constant pressure and temperature [14].

2. Experimental

The composition of the experimental steel obtained from a single steel plant is listed in Table 1. Metallographic specimens were polished to allow the observation of inclu-

Corresponding author: Fu-ming Wang E-mail: wangfuming@metall.ustb.edu.cn

sions in the cutting-wire steel. The compositions and morphologies of one hundred inclusions were analyzed using scanning electron microscopy (SEM) in conjunction with an energy dispersive spectrometer (EDS). The types and proportions of inclusions in the studied steel are shown in Table 2. The micrographs of complex inclusions are shown in Fig. 1.

Table 1. Chemical composition of the experimental steel sample wt%

C	Si	Mn	P	S	Al_s	Cr	T.O	Fe
0.83	0.18	0.50	0.0089	0.0080	0.0008	0.011	0.0022	Balance

Note: Al_s and T.O in Table 1 stand for the content of dissolved aluminum and the total content of oxygen, respectively.

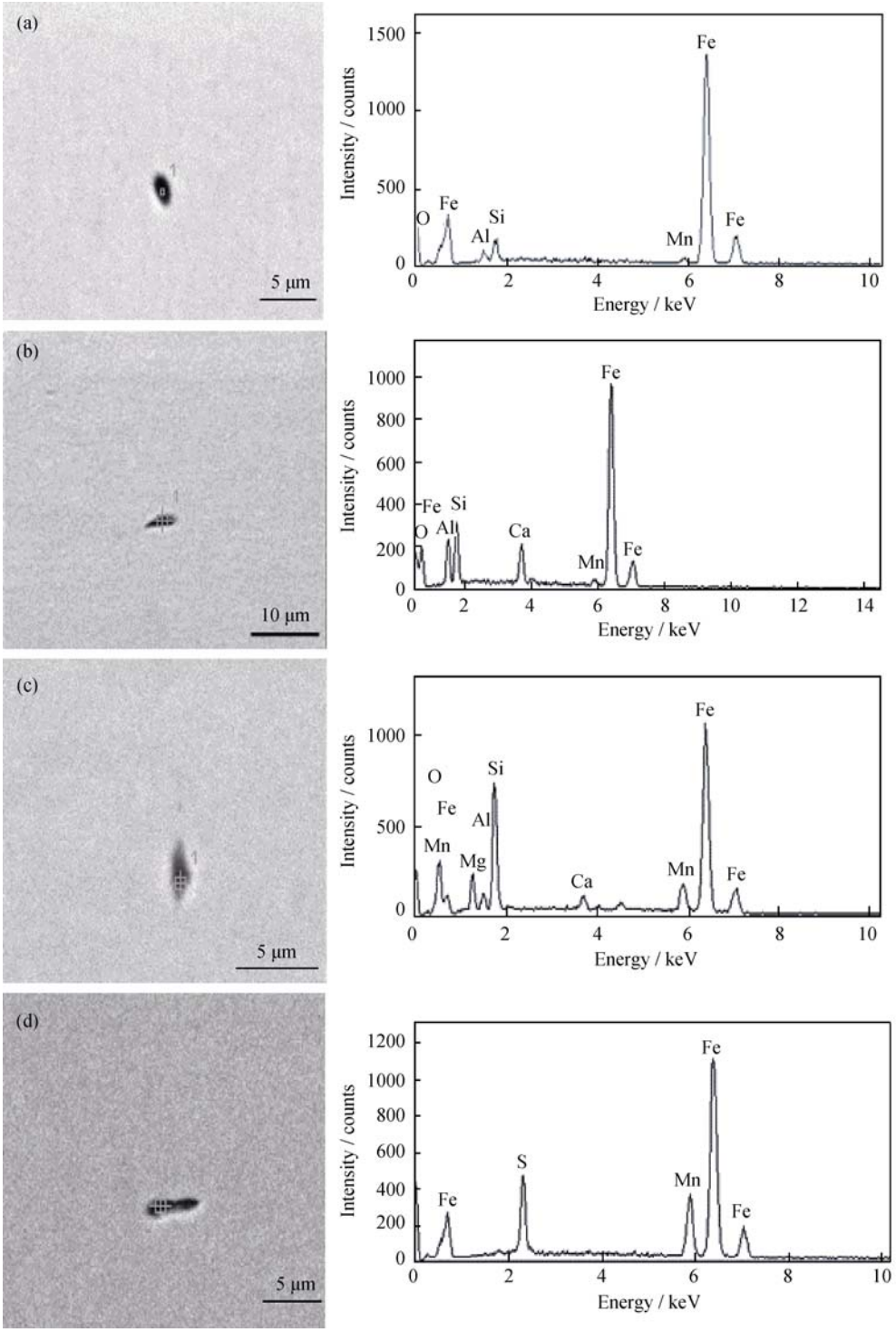

Fig. 1. Typical SEM morphologies and EDS spectra of inclusions: (a) Al_2O_3–SiO_2–MnO inclusion; (b) MnO–CaO–SiO_2–Al_2O_3 inclusion; (c) Al_2O_3–MnO–MgO–CaO–SiO_2 inclusion; (d) MnS inclusion.

Table 2. Proportion of all kinds of inclusions

Type of inclusions	Proportion of inclusions / %
MnS	83
Al_2O_3–SiO_2–MnO	4
MnO–CaO–SiO_2–Al_2O_3	9
Al_2O_3–MnO–MgO–CaO–SiO_2	4

As shown in Table 2, three kinds of complex oxide inclusions are present and the quaternary system MnO–CaO–SiO_2–Al_2O_3 accounts for a large proportion of the inclusions; this result is directly related to the drawing property of cutting-wire steel. Because the deformability of MnS inclusions is similar to that of the metal in the temperature range used in the steelmaking process, these inclusions are not taken into consideration.

To obtain the widest liquid region at 1400°C, the relationship between the composition of the MnO–CaO–SiO_2–Al_2O_3 inclusions and their melting point must be analyzed and the LMP (below 1400°C) zone in different phase diagrams should be compared. FactSage was used to calculate and draw 42 phase diagrams, including diagrams for MnO–CaO–SiO_2–Al_2O_3 with w(MnO) = 0%, 5%, 10%, 15%, 20%, 25%, 30%, 35%, and 40%, w(CaO) = 0, 5%, 10%, 15%, 20%, 25%, 30%, 35%, 40%, 45%, 50%, 55%, and 60%, w(SiO_2) = 0, 5%, 10%, 15%, 20%, 25%, 30%, 35%, 40%, 45%, and 50%, and w(Al_2O_3) = 0, 5%, 10%, 15%, 20%, 25%, 30%, 35%, and 40%.

3. Results and discussion

3.1. Effect of MnO content on the LMP zone

MnO, as the product of Mn/Si deoxidization, greatly affects the LMP zone in the MnO–CaO–SiO_2–Al_2O_3 system [15]. Control of the MnO content is therefore important to obtain a low liquidus temperature and low [O] content. The LMP zones at MnO contents of 0, 5wt%, 10wt%, 15wt%, 20wt%, 25wt%, 30wt%, 35wt%, and 40wt% were calculated using FactSage. The phase diagram at w(MnO) = 10% (w(Al_2O_3) + w(SiO_2) + w(CaO) = 100% and w(MnO)/(w(Al_2O_3) + w(SiO_2) + w(CaO)) = 10%) is shown in Fig. 2. The shaded regions indicate the liquidus zones at 1400°C.

The phase diagrams of the MnO–CaO–SiO_2–Al_2O_3 system with a MnO content that varied from 0 to 40wt% were computed. For each case, the ratio between the area of the liquidus zone at 1400°C and the whole area of the CaO–Al_2O_3–SiO_2 phase diagram is shown in Fig. 3. The liquidus zone (below 1400°C) extends significantly as the MnO content increases from 0 to 40wt%. Therefore, a reasonable enhancement of the MnO content favors the formation of LMP inclusions.

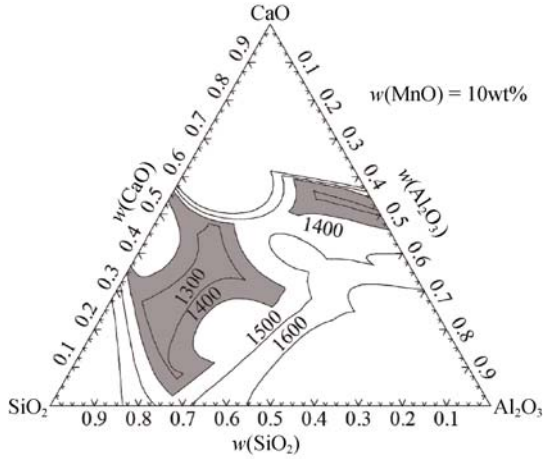

Fig. 2. Predicted liquidus surface of the MnO–CaO–SiO_2–Al_2O_3 system at 10wt% MnO.

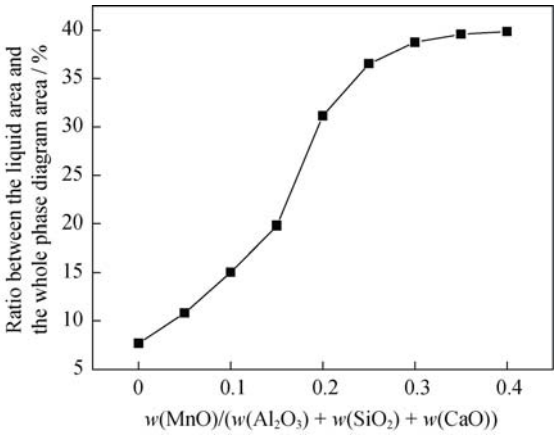

Fig. 3. Ratio between the liquid area at 1400°C and the area of the whole phase diagram at different MnO contents.

3.2. Effect of Al_2O_3 content on the LMP zone

After Mn/Si deoxidization, the content of manganese silicate, which is the product of deoxidization, is reduced by Al that originates from the ferroalloy; the brittle inclusion Al_2O_3 is generated simultaneously. The effect of Al_2O_3 content on the LMP zone was analyzed to avoid the deleterious effect of solid Al_2O_3. FactSage was used to calculate phase diagrams of the MnO–CaO–SiO_2–Al_2O_3 system with w(Al_2O_3) = 0, 5%, 10%, 15%, 20%, 25%, 30%, 35%, and 40%. A sample phase diagram at w(Al_2O_3) = 25% (w(MnO)+ w(SiO_2) + w(CaO) = 100% and w(Al_2O_3)/(w(MnO) + w(SiO_2) + w(CaO)) = 25%) is shown in Fig. 4. The shaded region represents the liquidus zone at 1400°C.

The phase diagrams of the MnO–CaO–SiO_2–Al_2O_3 system with an Al_2O_3 content that varies from 0 to 40wt% were calculated. The ratio between the area of the liquidus zone at

1400°C and the whole area of the CaO–MnO–SiO_2 phase diagram is displayed in Fig. 5 for all of the investigated Al_2O_3 contents. The liquidus zone (below 1400°C) increases with as the Al_2O_3 content increases from 0 to 25wt% and then decreases remarkably at greater Al_2O_3 contents. The widest liquid zone at 1400°C is therefore obtained at an Al_2O_3 content of 25wt%.

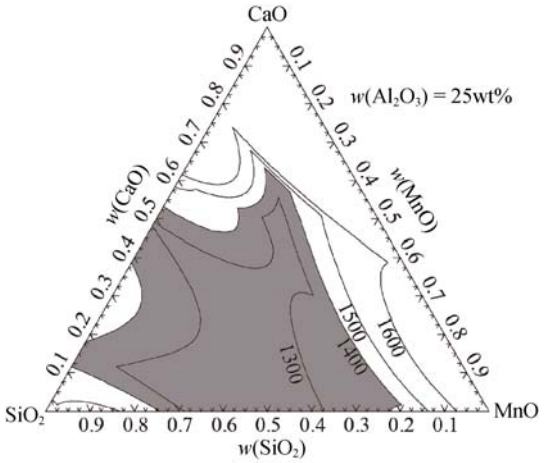

Fig. 4. Predicted liquidus surface of the MnO–CaO–SiO_2–Al_2O_3 system with 25wt% Al_2O_3.

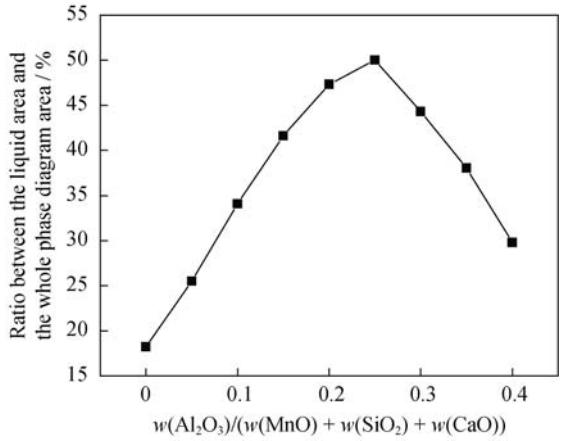

Fig. 5. Ratio between the liquid area at 1400°C and the whole phase diagram area at different Al_2O_3 contents.

3.3. Effect of CaO content on the LMP zone

Because CaO is a component of the MnO–CaO–SiO_2–Al_2O_3 system, an analysis of the effect of the CaO content on the liquidus temperature is necessary. FactSage was used to draw MnO–CaO–SiO_2–Al_2O_3 phase diagrams at w(CaO) = 0, 5%, 10%, 15%, 20%, 25%, 30%, 35%, 40%, 45%, 50%, 55%, and 60%. Fig. 6 presents the phase diagram at w(CaO) = 10% (w(MnO) + w(SiO_2) + w(Al_2O_3) = 100 wt%, and w(CaO)/(w(MnO) + w(SiO_2) + w(Al_2O_3)) = 10%) as an example. The shaded area represents the liquidus zone at 1400°C.

The phase diagrams of the MnO–CaO–SiO_2–Al_2O_3 system when the CaO content was varied from 0 to 60wt% were calculated. The ratio between the area of the liquidus zone at 1400°C and the whole area of the MnO–SiO_2–Al_2O_3 phase diagram is shown in Fig. 7 for each case. The liquidus zone (below 1400°C) increases sharply as the CaO content increases from 0 to 40wt% and then decreases in the CaO content range of 45wt% to 60wt%. Control of the CaO content within the range of 40wt% to 45wt% therefore favors the formation of LMP inclusions.

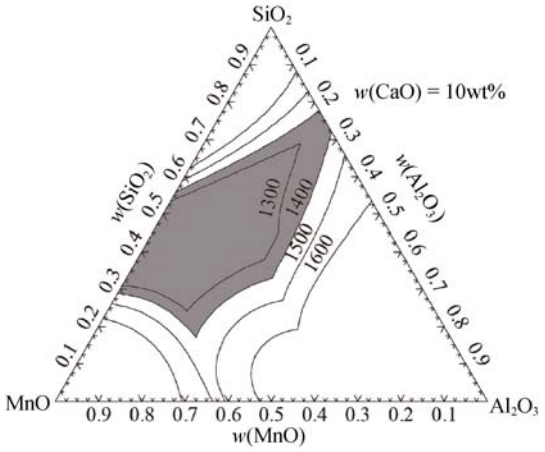

Fig. 6. Predicted liquidus surface of the MnO–CaO–SiO_2–Al_2O_3 system at 10wt% CaO.

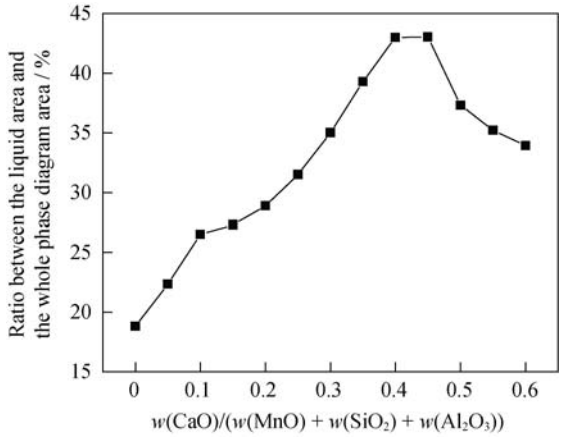

Fig. 7. Ratio between the liquid area at 1400°C and the whole phase diagram area at different CaO contents.

3.4. Effect of SiO_2 content on the LMP zone

As the product of Mn/Si deoxidization, SiO_2 significantly affects the LMP zone in the MnO–CaO–SiO_2–Al_2O_3 system, and the SiO_2 content of inclusions is largely dependent on the basicity of the slag. FactSage was used to construct MnO–CaO–SiO_2–Al_2O_3 phase diagrams at SiO_2 contents of 0, 5wt%, 10wt%, 15wt%, 20wt%, 25wt%, 30wt%, 35wt%, 40wt%, 45wt%, and 50wt%. Fig. 8 presents the phase diagram at w(SiO_2) = 30wt% as an example. The shaded region represents the liquidus zone at 1400°C.

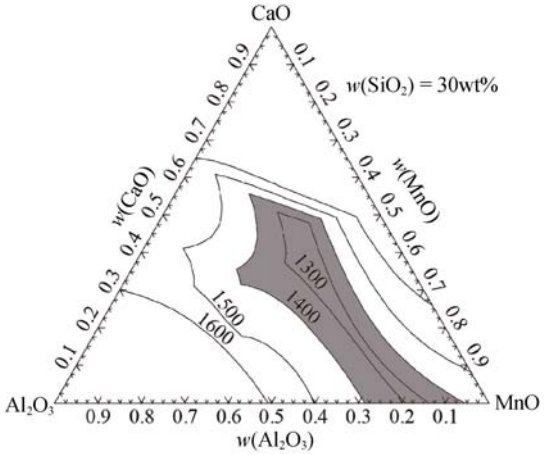

Fig. 8. Predicted liquidus surface of the MnO–CaO–SiO_2–Al_2O_3 system with 30wt% SiO_2.

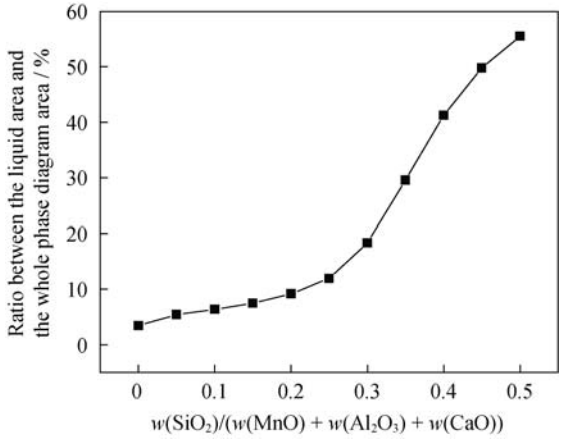

Fig. 9. Ratio between the liquid area at 1400°C and the whole phase diagram area at different SiO_2 contents.

The phase diagrams of the MnO–CaO–SiO_2–Al_2O_3 system with a SiO_2 content that varied from 0 to 50wt% were calculated. The ratio between the area of the liquid region at 1400°C and the whole area of the MnO–CaO–Al_2O_3 phase diagram is shown in Fig. 9 for each case. The liquidus zone at 1400°C is almost unchanged as the SiO_2 content increases from 0 to 30wt% and increases at higher SiO_2 contents. Therefore, the SiO_2 content should be controlled to exceed 30wt%.

3.5. Isometric (Iso)-activity diagrams of the MnO–CaO–SiO_2–Al_2O_3 system

In addition to calculating the phase diagrams, we also studied the activities of the oxide components in the MnO–CaO–SiO_2–Al_2O_3 system at an Al_2O_3 content of 25wt% using the FactSage software. The resulting iso-activity curves are shown in Fig. 10. The results demonstrate the following.

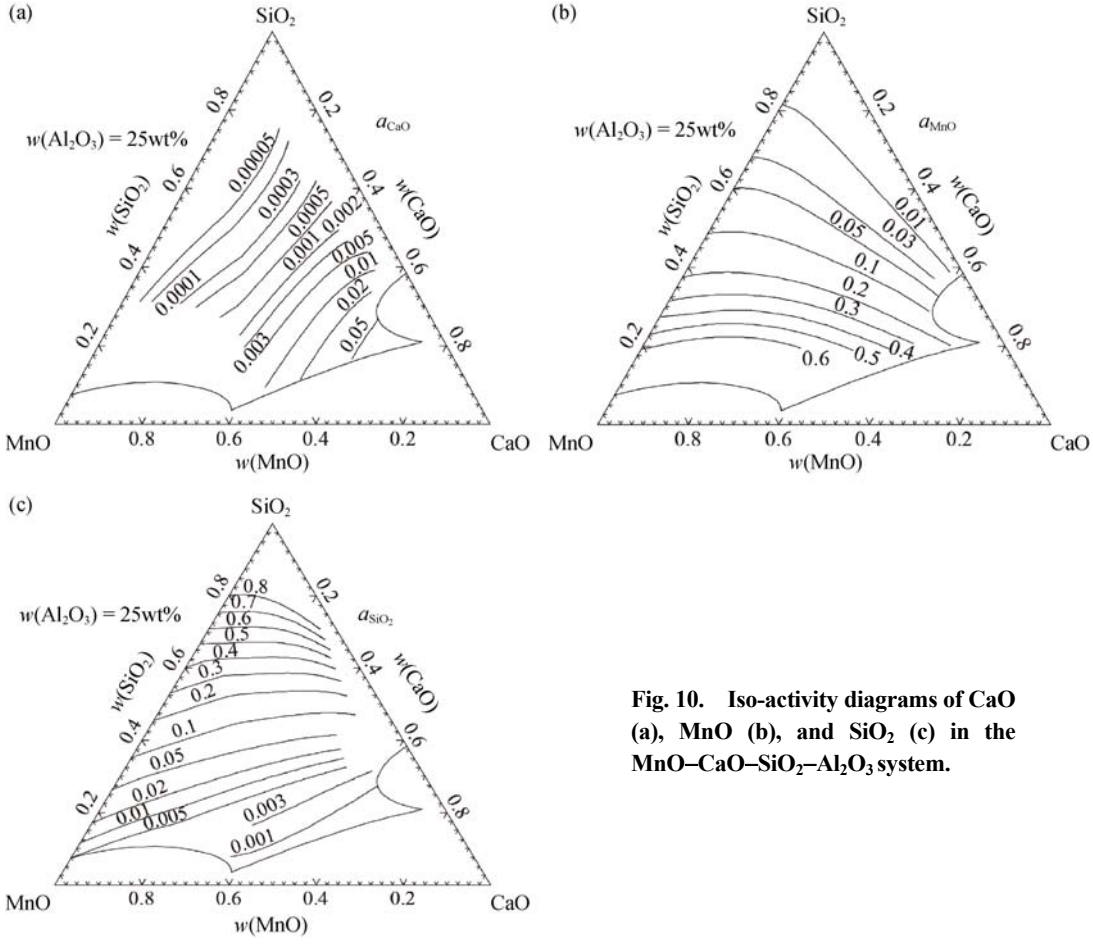

Fig. 10. Iso-activity diagrams of CaO (a), MnO (b), and SiO_2 (c) in the MnO–CaO–SiO_2–Al_2O_3 system.

(1) The activity of CaO increases with increasing CaO/SiO_2 ratio and decreases with increasing MnO content or SiO_2 content. In the liquidus zone, the activity of CaO varies from 0 to 0.05 and the controlled range is relatively small. (2) The activity of MnO increases with increasing CaO/SiO_2 ratio and decreases with increasing SiO_2 content. In the liquidus zone, the activity of MnO varies from 0.01 to 0.6 and the controlled range is large. (3) The activity of SiO_2 decreases with the increasing CaO/SiO_2 ratio. In the liquidus zone, the activity of SiO_2 varies within a large range of 0.001 to 0.8.

3.6. Control of composition in liquid steel

To obtain LMP MnO–CaO–SiO_2–Al_2O_3 inclusions, the composition of the steel must be well controlled. From the above calculation results, the MnO–CaO–SiO_2–25wt%Al_2O_3 (w(MnO) + w(SiO_2) + w(CaO) = 100% and w(Al_2O_3)/(w(MnO) + w(SiO_2) + w(CaO)) = 25%) system exhibits the largest liquid zone at 1400°C. Therefore, the [Al] and [O] contents in the liquid steel must be controlled to obtain LMP inclusions in the MnO–CaO–SiO_2–25%Al_2O_3 system. The [O] content in liquid steel with a composition of [C] = 0.83wt%, [Si] = 0.18wt%, and [Mn] = 0.50wt%, which was in equilibrium with the inclusions of the MnO–CaO–SiO_2–25%Al_2O_3 system at 1600°C, was calculated from the following equation:

$$[Si] + 2[O] = (SiO_2),$$

$$\Delta G_1^{\ominus} = -581900 + 221.8T, \text{ J/mol [16]} \quad (1)$$

where $\Delta G_1^{\ominus}$ is the Gibbs free energy at equilibrium and T is the absolute temperature.

The iso-[O]×10^6 curves were obtained by the iterative method, and the activity of SiO_2 was calculated using the FactSage software. The Wagner equation and the interaction coefficients of Sigworth and Elliott [16] were used to calculate the activity coefficients of silicon and aluminum. Finally, the iso-[O]×10^6 curves were drawn; the results are shown in Fig. 11.

The [Al] content in liquid steel being equilibrated with the MnO–CaO–SiO_2–25wt%Al_2O_3 system at 1600°C was calculated from Eq. (2) for [C] = 0.83wt%, [Si] = 0.18wt%, and [Mn] = 0.50wt% using the value of $\Delta G_2^{\ominus}$.

$$\frac{2}{3}(Al_2O_3) + [Si] = (SiO_2) + \frac{4}{3}[Al],$$

$$\Delta G_2^{\ominus} = 219400 - 35.7T, \text{ J/mol.} \quad (2)$$

The Wagner equation and the interaction coefficients of Suito and Inoue [1] were used to calculate the activity coefficient of aluminum. Finally, the iso-[Al]×10^6 curves were drawn; the results are shown in Fig. 12.

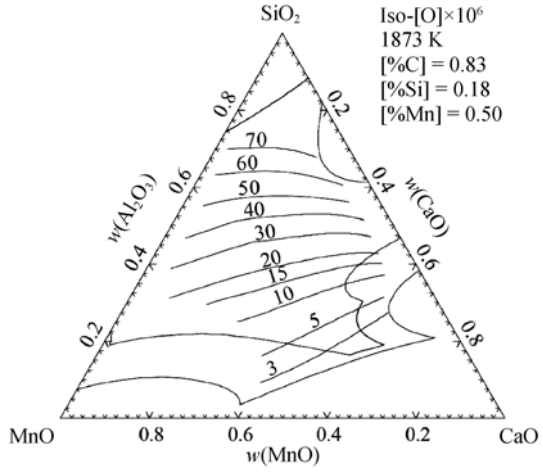

Fig. 11. Iso-[O]×10^6 curves in the MnO–CaO–SiO_2–Al_2O_3 system at 1600°C.

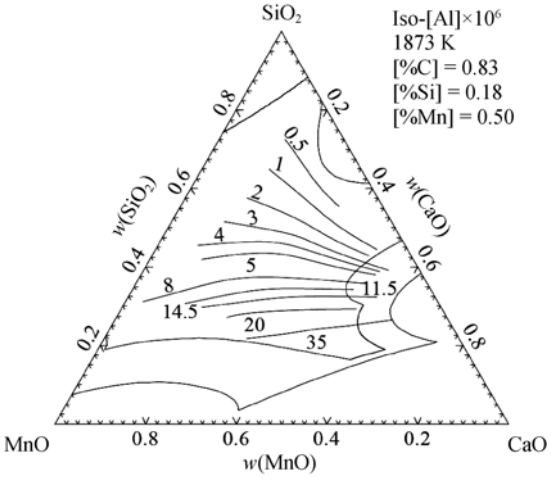

Fig. 12. Iso-[Al]×10^6 lines in the MnO–CaO–SiO_2–Al_2O_3 system at 1600°C.

The curves in Figs. 11 and 12 correspond to the inclusion composition in equilibrium with liquid steel with a composition of [C] = 0.83wt%, [Si] = 0.18wt% and [Mn] = 0.50wt%, which is similar to the composition of the cutting-wire steel. Given the required low [O] content, control of the [Al] and [O] contents in the liquid steel within a range of 0.5 × 10^{-6} to 1.0 × 10^{-5} and 3.0 × 10^{-6} to 5.0 × 10^{-5}, respectively, is a reasonable method for obtaining LMP inclusions.

To verify the above theoretical calculation results, the MgO and MnO contents in the inclusions were converted into CaO content and the processed compositions were overlaid onto the CaO–SiO_2–Al_2O_3 phase diagram. The distribution of the observed oxide inclusions is depicted in Fig. 13. The results reveal that most of the oxide inclusions are distributed in the LMP zone and that the calculation results

can guide actual production to some degree. The steel company from which the samples were acquired successfully controlled the composition control of inclusions.

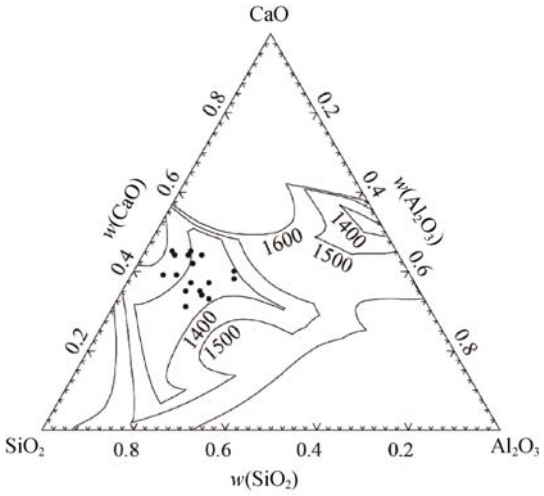

Fig. 13. Distribution of observed oxide inclusions in the $CaO–SiO_2–Al_2O_3$ phase diagram.

4. Conclusions

Inclusion control of cutting-wire steel was studied using the thermodynamic software FactSage. Forty-two phase diagrams were constructed to analyze the effect of each component oxide in the $MnO–CaO–SiO_2–Al_2O_3$ system on the liquidus temperature. The liquid steel composition was controlled to obtain LMP inclusions in the $MnO–CaO–SiO_2–25\%Al_2O_3$ system. The following conclusions were drawn:

(1) The LMP zone (at 1400°C) in the $MnO–CaO–SiO_2–Al_2O_3$ system is the largest when the Al_2O_3 content is 25wt%; the content of CaO should be controlled in the range of 40wt% to 45wt%.

(2) The activities of CaO, MnO, and SiO_2 should be restricted in the ranges of 0 to 0.05, 0.01 to 0.6, and 0.001 to 0.8, respectively.

(3) The [Al] and [O] contents in the liquid steel should be controlled in the ranges of 0.5×10^{-6} to 1.0×10^{-5} and 3.0×10^{-6} to 5.0×10^{-5}, respectively, to obtain LMP inclusions in the $MnO–CaO–SiO_2–25\%Al_2O_3$ system.

References

[1] H. Suito and R. Inoue, Thermodynamics on control of inclusions composition in ultra-clean steels, *ISIJ Int.*, 36(1996), No. 5, p. 528.

[2] J.H. Liu, H.J. Wu, Y.P. Bao, and M. Wang, Inclusion variations and calcium treatment optimization in pipeline steel production, *Int. J. Miner. Metall. Mater.*, 18(2011), No. 5, p. 527.

[3] M. Gagné and E. Thibaultt, Control of inclusion characteristics in direct cast steel billets, *Can. Metall. Q.*, 38(1999), No. 5, p. 311.

[4] L.F. Wang, X.J. Zhuo, J.M. Zhang, and X.H. Wang, Controlling inclusion composition in steelmaking process for tire cord steel, *J. Univ. Sci. Technol. Beijing*, 25(2003), No. 4, p. 308.

[5] K. Kume, K. Morita, T. Miki, and N. Sano, Activity measurement of $CaO–SiO_2–AlO_{1.5}–MgO$ slags equilibrated with molten silicon alloys, *ISIJ Int.*, 40(2000), No. 6, p. 561.

[6] H.T. Wang, F.M. Wang, Z.B. Xu, and L.L. Jin, Composition control of $CaO–MgO–Al_2O_3–SiO_2$ inclusion in tire cord steel: a thermodynamic analysis, *Steel Res. Int.*, 79(2008), No. 1, p. 25.

[7] H.G. Zheng and W.Q. Chen, Formation of $CaO{\cdot}TiO_2–MgO{\cdot}DAl_2O_3$ dual phase inclusion in Ti stabilized stainless steel, *J. Univ. Sci. Technol. Beijing*, 13(2006), No. 1, p. 16.

[8] Y.B. Kang, H.S. Kim, J. Zhang, and H.G. Lee, Practical application of thermodynamics to inclusions engineer in steel, *J. Phys. Chem. Solids*, 66(2005), No. 2-4, p. 219.

[9] X.J. Zhuo, Y.Q. Wang, X.H. Wang, and H.G. Lee, Thermodynamic calculation and MnS solubility of Mn–Ti oxide formation in Si–Mn–Ti deoxidized steel, *J. Iron Steel Res. Int.*, 17(2010), No. 2, p. 10.

[10] L.L. Jin, H.T. Wang, Z.B. Xu, and F.M. Wang, Control on low melting point area in a $CaO–SiO_2–Al_2O_3–MnO$ system, *J. Univ. Sci. Technol. Beijing*, 29(2007), No. 6, p. 574.

[11] Y.B. Kang, I.H. Jung, S.A. Decterov, A.D. Pelton, and H.G. Lee, Critical thermodynamic evaluation and optimization of the $CaO–MnO–SiO_2$ and $CaO–MnO–Al_2O_3$ systems, *ISIJ Int.*, 44(2004), No. 6, p. 965.

[12] S.F. Wang and H. Ma, Effect of deformability of $CaO–MgO–SiO_2–Al_2O_3$ series inclusion on breakage rate of tire cord steel in processing, *Spec. Steel,* 33(2012), No. 3, p. 32.

[13] X.J. Zhuo, X.H. Wang, W.J. Wang, and H.G. Lee, Thermodynamic calculations and experiments on inclusions to be nucleation sites for intragranular ferrite in Si–Mn–Ti deoxidized steel, *J. Univ. Sci. Technol. Beijing*, 14(2007), No. 1, p. 14.

[14] C.W. Bale, P. Chartrand, S.A. Degterov, G. Eriksson, K. Hack, R.B. Mahfoud, J. Melançon, A.D. Pelton, and S. Petersen, FactSage thermochemical software and databases, *Calphad,* 26(2002), No. 2, p. 189.

[15] Y.B. Kang and H.G. Lee, Inclusions chemistry for Mn/Si deoxidized steels: thermodynamic predictions and experimental confirmations, *ISIJ Int.*, 44(2004), No. 6, p. 1006.

[16] G.K. Sigworth and J.F. Elliott, The thermodynamics of liquid dilute iron alloys, *Met. Sci.*, 8(1974), No. 1, p. 298.